Effects of Rotation on Convective Plumes from Line Segment Sources*

J. W. LAVELLE

NOAA Pacific Marine Environmental Laboratory, Seattle, Washington

D. C. SMITH IV

Institute of Marine Sciences, University of California, Santa Cruz, Santa Cruz, California

(Manuscript received 29 December 1994, in final form 7 August 1995)

ABSTRACT

Effects of rotation on finite-length line plumes are studied with a three-dimensional nonhydrostatic numerical model. Geophysical convection with this source geometry occurs, for example, as the result of fissure releases of hot hydrothermal fluids at the seafloor from terrestrial release of hot gases and ash during volcanic activity along fissures and in the descent from the sea surface of brines formed during freezing of ice leads at high latitudes. Here the model treats the case of a starting plume of dense fluid descending into a rotating environment. Results are compared with laboratory experiments so that the validity of the model, particularly the nonlinear subgrid-scale mixing formulation, might first be established. Differences in plumes caused by varying rotation rate, Ω, and buoyancy flux, B_0, are the primary focus, with experiments in fluid of depth h spanning a convective Rossby number $[B_0^{1/3}/(2\Omega h)]$ of 0.01–1.0. Rotation initiates spiraling of the descending plumes but it has little effect on the speed of plume descent; the latter depends on the strength of turbulent mixing. Low rotation rates allow the descending plume cap to be broad and the stem to be narrow. Higher rotation rates retard the lateral spread of the plume cap and widen the plume stem. Updraft at the stem edge is very much larger at higher rotation rates, and that appears to be instrumental in determining stem and cap width. Values of turbulent mixing coefficients within the plume are dependent on B_0 but not on Ω. Thus rotational effects on turbulence are not needed to account for differences in plume structure arising solely from Ω variation. Agreement between model and laboratory results did not occur without a nonlinear time- and space-dependent subgrid-scale mixing parameterization, suggesting that model applications to convective geophysical problems identified above require the same.

1. Introduction

Convection from line segment sources of buoyancy occur in a number of geophysical settings. At the seafloor, fissure release of hot hydrothermal fluids accompanying seismic and magmatic events are the likely cause of the benthic water-column property anomalies at submarine ridge crests known as megaplumes (e.g., Embley et al. 1995; Lavelle 1995; Baker et al. 1995). At high latitudes, lineal convective descent of brine from the sea surface occurs during freezing of long, narrow ice leads (e.g., Smith and Morison 1993). In the coastal environment, buoyant waste water is commonly discharged at depth from a linear array of diffusers (e.g., Roberts 1979). In the terrestrial environment volcanic activity along fissures can release hot gases and ash that rise high into the atmosphere (Strothers 1989; Woods 1993). Beyond source geometry, each of these shares the fact that the convection occurs in a rotating environment. Only recently have effects of rotation on convective plumes from line segment sources come under examination (Fernando and Ching 1993). To complement that laboratory study, we here examine rotating convection from line segment sources using a three-dimensional nonhydrostatic numerical model.

A linchpin in any numerical description of convection is the treatment of subgrid-scale turbulence. Though many subgrid-scale parameterizations and some comparative studies for line plumes are available (e.g., Drake et al. 1974; Lipps 1977; Tag et al. 1979), few appear to be tested in the context of measured convection where rotation is important. In this paper, a convection model for a line segment source is tested against laboratory results (Fernando and Ching 1993) as a way of checking the fidelity of the nonlinear subgrid-scale parameterization employed. The comparison involves studying effects of variable rotation rate and buoyancy flux on plume distributions.

* NOAA/Pacific Marine Environmental Laboratory Contribution Number 1608.

Corresponding author address: Dr. J. W. Lavelle, NOAA-PMEL, 7600 Sand Point Way, NE, Seattle, WA 98115.
E-mail: lavelle@pmel.noaa.gov

Several other recent laboratory studies have undertaken the study of effects of rotation on convective plumes but not in line or line segment source geometry. Maxworthy and Narimousa (1994) studied rotating convection in the laboratory for a distributed circular source. Helfrich (1994) studied buoyant point source thermals in both unstratified and stratified rotating environments. Jones and Marshall (1993) undertook a numerical study of rotating convection in a geometry similar to that of Maxworthy and Narimousa (1994), but only constant turbulent mixing coefficients were employed. Effects of rotation on turbulence itself, rather than on plumes, have been also given considerable attention in recent years. These include laboratory studies of Fernando et al. (1991) on a developing mixed layer, numerical studies of Raasch and Etling (1991) on convective boundary layers, and those of Bardina et al. (1985) on direct numerical simulations of turbulence decaying downstream of a rotating grid. References to work on line plumes without rotation can be found in Ching et al. (1993), who studied the effectiveness of a density interface in stopping the penetration of a line segment plume of brine convecting downward into a two-layer stratified but nonrotating tank. The distinction between line and line segment plumes is clear; when source length is finite, end effects are important and the problem is three-dimensional.

This analysis makes these points: The likeness of model and laboratory results depends on the subgrid-scale mixing parameterization, even though model spatial resolution is reasonably high. Spatially and temporally invariant mixing coefficients, even if relatively small, do not adequately represent effects of unresolved motion. Effects of rotation on plumes do not require rotational effects on turbulence; changes in nonchaotic advective motion caused by rotation suffice to lead to effects observed. Both results have implications for modeling geophysical flows.

2. Model formulation

The model describes the nonhydrostatic response of an incompressible fluid in the Boussinesq approximation to a suddenly imposed, localized buoyancy source. Together with the equation of state of seawater (Fofonoff and Millard 1983), model equations are the following:

$$\frac{\partial}{\partial t}\mathbf{u} + \mathbf{u}\cdot\nabla\mathbf{u} = -\nabla p/\rho_0 - 2\boldsymbol{\Omega}\times\mathbf{u} + \nabla\cdot A\nabla\mathbf{u} - \mathbf{k}g\rho/\rho_0 \quad (1)$$

$$\nabla\cdot\mathbf{u} = 0 \quad (2)$$

$$\frac{\partial}{\partial t}(\theta, S) + \mathbf{u}\cdot\nabla(\theta, S) = \nabla\cdot K\nabla(\theta, S) + Q_{\theta,S} \quad (3)$$

$$A_H = A_I + A_{H\min} \quad (4)$$

$$A_V = A_I + A_{V\min} \quad (5)$$

$$A_I = (C_S l_S)^2 (2\tilde{S}_{ij}\tilde{S}_{ij})^{1/2}\left(1 - \frac{\mathrm{Ri}}{\mathrm{Pr}}\right)^{1/2}, \quad i, j = x, y, z, \quad \mathrm{Ri} \leqslant \mathrm{Pr} \quad (6)$$

$$A_I = 0, \quad \mathrm{Ri} > \mathrm{Pr} \quad (7)$$

$$\mathrm{Ri} = -g\rho_0^{-1}(\partial\rho/\partial z)(2\tilde{S}_{ij}\tilde{S}_{ij})^{-1}, \quad i, j = x, y, z \quad (8)$$

$$\tilde{S}_{ij} = \frac{1}{2}(\partial u_i/\partial x_j + \partial u_j/\partial x_i), \quad i, j = x, y, z \quad (9)$$

$$K_j = A_j/\mathrm{Pr}, \quad j = H, V, \quad (10)$$

where t is time; $\mathbf{u}$ consists of u, v, and vertical w (positive upward) components; p is pressure; ρ is density; ρ_0 (998.21 kg m^{-3}) a reference density; g (9.81 m s^{-2}) the acceleration of gravity; and $\boldsymbol{\Omega}$ the rotation vector, which here takes the form $\boldsymbol{\Omega} = |\Omega|\mathbf{k}$. Potential temperature θ and salinity S depend on the rates of discharge of heat Q_H, via $Q_\theta = Q_H/(\rho_0 C_P)$, and salt Q_S. Equations (1)–(3) are conservation equations for momentum, mass (given fluid incompressibility), and heat (salt). Retention of all terms in the vertical force balance make the model nonhydrostatic. The viscosity tensor A and the diffusivity tensor K are time and space dependent.

Equations (4)–(10) constitute the turbulence closure submodel. The horizontal and vertical components of the mixing tensors $A_{H\text{ or }V}$ [and $K_{H\text{ or }V}$ via Eq. (10)] are each composed of two parts: an isotropic (A_I) mixing coefficient and either horizontal ($A_{H\min}$) or vertical ($A_{V\min}$) background terms [Eqs. (4)–(5)]. The isotropic mixing coefficient A_I [Eqs. (6)–(7)] is made to depend on fluid shear [$\tilde{S}_{ij}$, here given in Cartesian form, Eq. (9)], on the shear Richardson number [Ri, Eq. (8)], on Prandtl number [Pr, Eq. (10)], and on the turbulence length scale (l_S) and Smagorinsky (C_S) constant Eq. (6). If Ri were zero, Eq. (6) would reduce to a form originating with Smagorinsky (1963); it stems from an assumed local balance in the turbulence kinetic energy (TKE) equation between shear production and turbulence dissipation. When buoyancy production or dissipation is added to the local TKE balance, the Ri-dependent factor becomes part of the formulation (Lilly 1962). Note that the mixing terms have no explicit dependence on rotation. The reason is that in forming total TKE terms involving Ω sum to zero.

Smagorinsky–Lilly mixing, with or without the Ri-dependent factor, is in widespread use (e.g., Clark and Farley 1984). Subgrid-scale mixing of this type is frequently used in large eddy simulations (LES) (e.g., Galperin and Orsag 1993; Mason 1994). Background mixing terms [Eqs. (4)–(5)], presumed to be small, have here been added to A_I to ensure a modest amount of mixing in regions without shear, for example, away from the plume region, where A_I will be zero.

Simulations were made of a salt-laden plume falling through a rotating tank of fresh water held at constant temperature (20°C). Length scales, source buoyancies B_0, and rotation rates Ω were chosen to be comparable to those of the laboratory experiments (Fernando and Ching 1993). Thus, equations were solved in a Cartesian domain 30 cm × 60 cm × 30 cm; Δx, Δy, Δz were 0.25, 2.0, and 0.5 cm respectively. Time steps Δt were either 0.01 or 0.005 s depending on B_0. Source length l and width b were 15 and 0.75 cm respectively; computational constraints prevented a smaller b. Simulations were terminated when the plume had penetrated to slightly more than $0.5h$, where h is maximum depth, and before effects on the plume of the walls and bottom of the tank were significant.

Equations were finite differenced and solved using methods analogous to those described in Lavelle and Baker (1994), save for forward time differencing, which was here deemed suitable for the short integration periods involved. Null gradients were imposed at boundaries for all variables, exceptions being zero normal velocities and pressure gradients prescribed in the manner of Harlow and Welch (1965). Parameter values were typically these: $A_{H\min} = A_{V\min} = 1 \times 10^{-6}$ m^2 s^{-1}, a value in the range of molecular viscosity; $C_S = 0.2$; and Pr, the ratio of turbulent viscosity to diffusivity, was given the value 1.0. The mixing length l_S, about which more will be said later, was given a magnitude comparable to b in all cases. Values for l_S, C_S, and Pr are not uniquely assignable, but values selected here are in ranges commonly used, and the combination chosen led to good simulation of laboratory results. Sensitivity of plume results to variations of these parameters can be found, in part, in a study of axisymmetric plumes by Lavelle and Baker (1994).

Results of 12 experiments are reported here: B_0 took values of 2×10^{-6}, 40×10^{-6}, or 200×10^{-6} m^3 s^{-3}, and Ω was given values of 0.1, 0.5, 1.0, or 1.57 s^{-1}. These ranges are larger by a factor of 1.5 to 2 than those covered by Fernando and Ching (1993). For nominal molecular viscosity ν and molecular diffusivity κ values of 1×10^{-6} m^2 s^{-1} [values like those assigned $A_{H\min}$ and $A_{V\min}$ (and $K_{H\min}$ and $K_{V\min}$ since Pr = 1.0)], and for fluid depth h of 30 cm, B_0 and Ω values result in flux Rayleigh numbers, $\mathrm{Ra} = B_0 h^3/(\kappa^2\nu)$, of $5 \times 10^{10} < \mathrm{Ra} < 5 \times 10^{12}$ and Taylor numbers, $\mathrm{Ta} = (2\Omega)^2 h^4/\nu^2$, of $3 \times 10^8 < \mathrm{Ta} < 8 \times 10^{10}$. The advice of Maxworthy and Narimousa (1994) that for turbulent flows these parameters have dubious meaning should not be overlooked, however. Raasch and Etling (1991), in studying convective boundary layers, defined a convective Rossby number, $\mathrm{Ro}_C = w^*/(fh)$, using a characteristic vertical convection velocity w^* and the depth of the convection region h. A convection Rossby number for a line plume in a depth (h) limited region can, in analogy, be defined as $\mathrm{Ro}_C = B_0^{1/3}/(2\Omega h)$ if the frontal velocity w_P of the descending plume edge is used for w^* because, as will be shown, $w_P \sim B_0^{1/3}$. For experiments reported here $0.01 < \mathrm{Ro}_C < 1.0$. Note that these Ra and Ro_C definitions pertain to linear sources, for which B_0 has dimensions of L^3/T^3. Maximum computational Reynolds numbers, for example, $(\nu\Delta y)/A_{H,V}$, were $O(100)$ in the along-source direction.

3. Results and discussion

Figure 1, showing the $S = 0.1\%$ isosurface of a plume from one of the calculations ($B_0 = 40 \times 10^{-6}$ m^3 s^{-3}, $\Omega = 0.5$ s^{-1}) as $t = 4.5$ s, orients the descriptions that follow. The line segment source is oriented along the y axis and is centered at horizontal coordinates (0, 0); the transverse direction is x, and z is positive upward. While early in the evolution of the plume in terms of the rotation, the figure shows the stem beginning to twist: in the foreground, the curved plume stem tends to the right of the linear source (Ω is positive), while in the background the opposite is true. Cap growth is greater transversely than longitudinally. As the plume descends, the plume cap grows in breadth subject to counterrotating vortices located therein on either side of the stem. In the case shown, the penetration depth, as indicated by the $S = 0.1‰$ isopleth at $x = y = 0$ is ~16 cm and the width at $y = 0$ is 8.8 cm. Fernando and Ching (1993) describe laboratory line segment plumes as having cylindrical caps and wedge-shaped tails. The required width of the model brine source apparently precludes a wedge-shaped tail, but the plume cap, for cases having smaller rotation rates is reasonably cylindrical.

More detailed distributions for the same plume are shown in Fig. 2. Cross sections in two vertical planes ($y = 0$ and $y = -5$ cm, Figs. 2a,b) show the plume cap

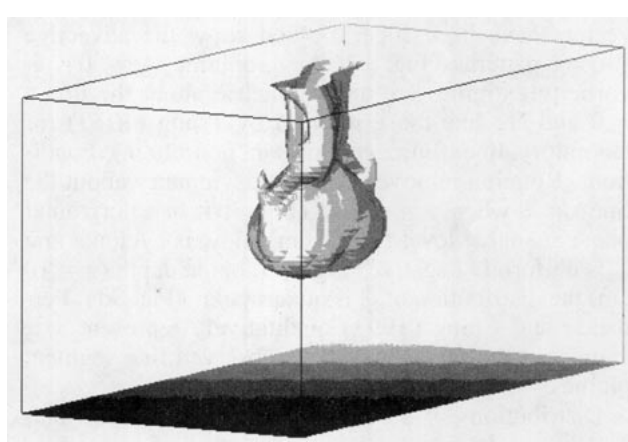

FIG. 1. The $S = 0.1‰$ isosurface of a negatively buoyant model plume descending in a rotating tank. For this case, $B_0 = 40 \times 10^{-6}$ m^3 s^{-3} and $\Omega = 0.5$ s^{-1}. Time is 4.5 s. The source is oriented along the y axis and rotation is cyclonic about the vertical (positive upward).

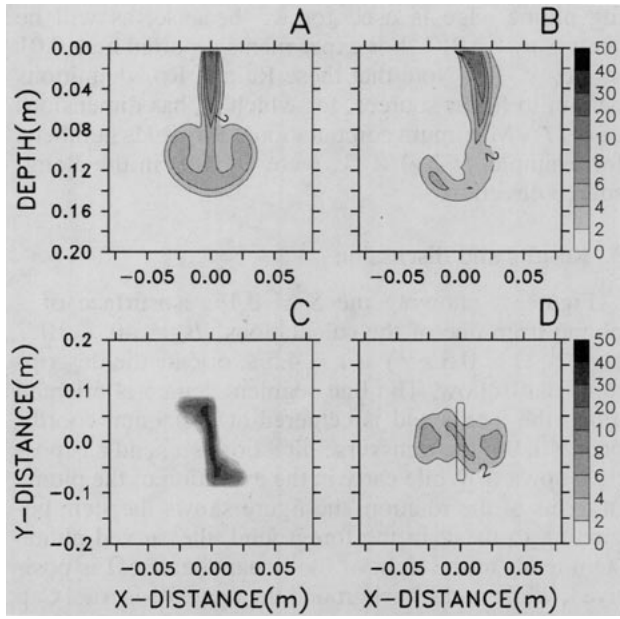

FIG. 2. Snapshots at $\Omega t = 2.3$ of salinity (‰) in a plume in (a) the x–z plane at $y = 0$; (b) in the x–z plane at $y = -5$ cm; (c) in the x–y plane at $z = 0$; (d) in the x–y plane at $z = 10$ cm where the centered rectangular contour represents the source size and orientation. In this case $B_0 = 40 \times 10^{-6}$ m^3 s^{-3} and $\Omega = 0.5$ s^{-1}. Scale differences in horizontal coordinates exaggerate the twisting of the plume.

considerably broader than the stem. Near the proximal end of the plume ($y = -5$ cm), the displacement caused by Coriolis force is clear. Salinities on two horizontal planes ($z = 0$ and $z = 10$ cm) show twisting in the plume stem (Fig. 2c) and a plume cap (Fig. 2d) that has broadened more in the direction transverse to the source axis than longitudinally.

Corresponding distributions of relative vorticity about the y and z axes, ζ_y and ζ_z, onto which velocity vectors have been superimposed show the advective stirring patterns (Fig. 3). At midplume ($y = 0$), ζ_y vorticity extremes are antisymmetric about the line $x = 0$ and are like those inferred by Tsang (1970) for laboratory line source plumes in nonrotating conditions. Rotation removes the ζ_y antisymmetry about the line $x = 0$ when $y = -5$ cm (Fig. 3b). In a horizontal plane at source level ($z = 0$ cm), flow is cyclonic and ζ_z is uniformly negative (Fig. 3c), but at depth ($z = 10$ cm) the distribution of ζ_z is quadrupolar (Fig. 3d). Fernando and Ching (1993) qualitatively represent a ζ_z couplet at the far ends of their observed line segment plumes.

Distributions of salinity across the plume at midlength ($y = 0$) for identical times ($t = 4.55$ s) for four separate experiments ($B_0 = 40 \times 10^{-6}$ m^3 s^{-3}, while $\Omega = 0.1$, 0.5, 1.0, and 1.57 s^{-1}) show substantial qualitative changes in plumes as the result of rotation (Fig. 4). Low rotation rates allow the descending plume cap to be relatively broad and the stem near the source to remain narrow. High rotation rates retard the lateral spread of the plume cap and result in wider plume stems, the causes of which we will return to later. Figure 4 show that penetration depths h_P are essentially identical. The following analysis shows more incisively that both h_P and w_P, the plume penetration speed, have no dependence on Ω.

Fernando and Ching (1993) chose to demonstrate the time dependence of plume penetration depth by plotting nondimensional $\tilde{h}_P = h_P/(B_0^{1/3}/\Omega)$ versus Ωt. Their results showed that $\tilde{h}_P$ was highly correlated with Ωt, but $\tilde{h}_P$ had no additional B_0 or source length dependence. To examine the model results in the same regard $\tilde{h}_P$, as delineated by the 0.1% salinity isopleth at $x = y = 0$, was sampled five or more times in each of the 12 numerical experiments. When plotted using the same nondimensional variables, model results (Fig. 5) show the same high correlation. The unweighted least-squares best fit line through the origin has a slope α of 0.96, slightly less than the slope of 1.2 reported by Fernando and Ching (1993). It is clear that the correlation of the two variables in Fig. 5 simply means that $h_P = \alpha B_0^{1/3} t$, where t is the absolute time, and if there is additional Ωt dependence, it is weak indeed; thus penetration depth grows linearly with time, depends on B_0, and has no Ω dependence. As a consequence, penetration speed $w_P = d(h_P)/dt = \alpha B_0^{1/3}$ also is independent of Ω but has the same 1/3 power dependence on B_0.

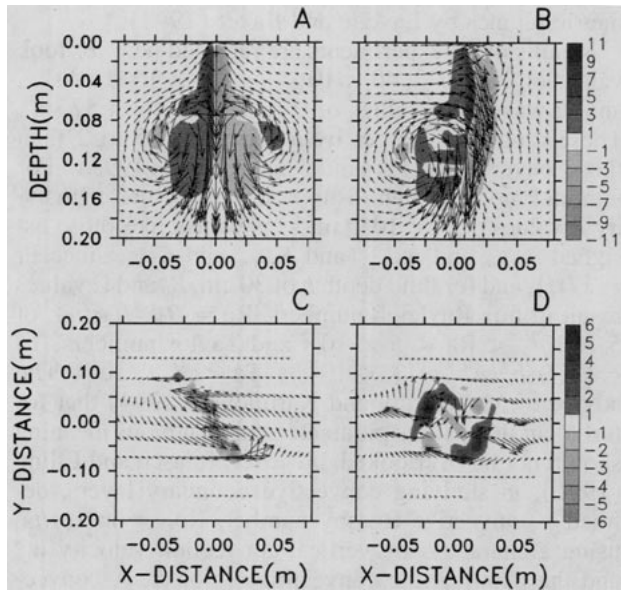

FIG. 3. Relative vorticity (shaded) in units of inverse seconds and velocity vectors in the same planes and for the same plume as in Fig. 2. Vectors have been thinned by two in each direction for this figure.

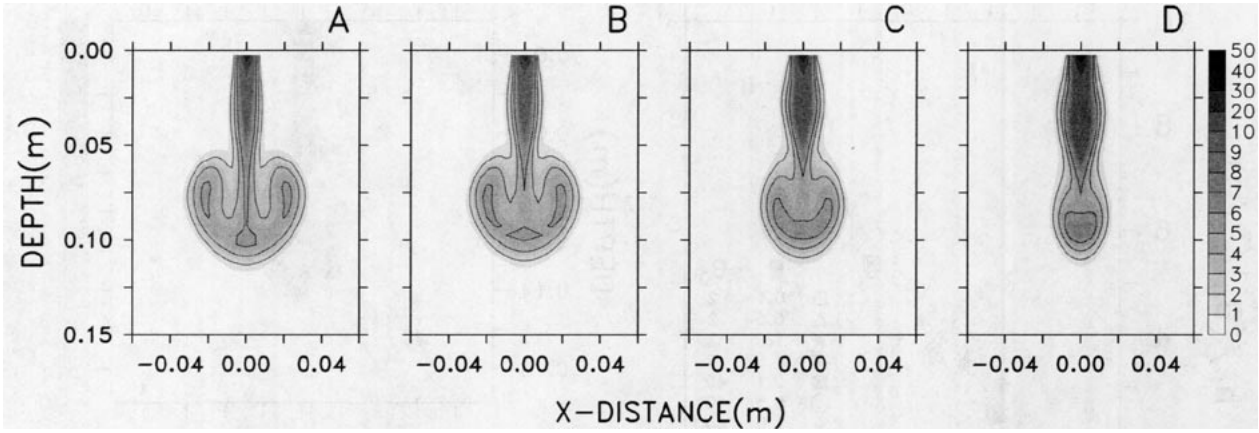

FIG. 4. Effects of rotation on brine plumes with identical buoyancy flux. In all examples, $t = 4.5$ s, $B_0 = 40 \times 10^{-6}$ m^3 s^{-3}, and plumes are sampled in a plane ($y = 0$) transverse to the long axis of the plume. Line contours are of salinity at 2‰, 4‰, and 6‰. Rates of rotation Ω are (a) 0.1 s^{-1}, (b) 0.5 s^{-1}, (c) 1.0 s^{-1}, and (d) 1.57 s^{-1}.

While the results of the Fernando and Ching (1993) experiments suggest a linear relationship between $h_P/(B_0^{1/3}/\Omega)$ and Ωt, the linearity of the model data in Fig. 5 was not serendipitous. For fixed B_0 and Ω, model results showed $\tilde{h}_P$ to be dependent on the magnitude of A_I [Eqs. (4)–(5)], more specifically on the coefficient product $C_S l_S$ [Eq. (6)] since Pr is held fixed. As an example of this dependence, and to underscore the fact that results for nonrotational cases must be similar to cases at low rotation rates (e.g., $\Omega = 0.1$ s^{-1}) over short initial time intervals, we have compared two nonrotational cases ($\Omega = 0$, $B_0 = 40 \times 10^{-6}$ m^3 s^{-3}) when $C_S = 0$ and $C_S = 0.2$. In the first case, mixing occurs at background mixing levels only [Eqs. (4)–(7)]; that magnitude is 10^{-6} m^2 s^{-1}, 36 times less than the maximum $A_H = A_V$ that occurs within the plume when $C_S = 0.2$.

Results of those calculations (Fig. 6) in the plane $y = 0$, for example, show that penetration depths and thus penetration speeds of the two plumes differ by nearly a factor of 2. Maximum plume width is also very different. Maximum ν and w velocities more than double when $C_S = 0$. Clearly, the strength of mixing within the plume itself makes a difference; the experimental data of Fernando and Ching (1993) at low rotation rates imply that the second ($C_S = 0.2$) result is to be preferred to the first ($C_S = 0$). The second case is preferred philosophically as well because turbulent mixing within and well beyond the plume should have different intensities, and only spatially variable coefficients can account for the inhomogeneity. Because the region of increased mixing grows in time, mixing coefficients must be temporally variable too. Of course, it may be possible to find a single fixed value for mixing coefficients that could duplicate the results coming from the use of a Smagorinsky mixing formulation (Fig. 6, $C_S = 0.2$) but that would either mean having to calculate first with the variable mixing formulation and subsequently finding an average A (e.g., Mason 1994) or having to discover an appropriate constant A on a case-by-case basis. Moreover, the end result will be having unnecessarily, or perhaps even unrealistically, large mixing coefficients in regions outside the plume that are essentially unperturbed by the convection.

Results of the experiments for plumes undergoing rotation showed similar results with regard to mixing. Smaller values of $C_S l_S$ allowed the plumes of intermediate (40×10^{-6} m^3 s^{-3}) and large (200×10^{-6} m^3 s^{-3}) B_0 to penetrate too quickly into the interior, whereas a fluid made too viscous by too large a $C_S l_S$ did not penetrate quickly enough and the result was data pairs that plotted above or below the best-fit line of Fig. 5. For the case of smallest B_0 that effect was not so apparent, primarily because the A_I contribution to A_H and A_V [Eqs. (4)–(5)] was not much larger than the $A_{H\min} = A_{V\min}$ contribution.

The key to making $\tilde{h}_P$ versus Ωt model results collinear (Fig. 5) was careful selection of the magnitude of $C_S l_S$ [Eq. (6)], more precisely l_S, since we chose to fix C_S at 0.2 (e.g., Smagorinsky 1993). For LES calculations of homogeneous flows it is common (e.g., Mason 1994) to take l_S proportional to a grid length scale, $\Delta = (\Delta x \Delta y \Delta z)^{1/3}$, but the same prescription is known to be inadequate for LES calculations of boundary-layer shear flows (e.g., Mason and Brown 1994). For inhomogeneous sheared flows involving jets, buoyant jets, or plumes, it is consequently not unreasonable to expect that l_S be unequal in size to Δ. Previous results with point source axisymmetric plumes using the Smagorinsky form for viscosity/diffusivity (Lavelle and Baker 1994) had shown, for fixed B_0, that the invariance of plume rise height under changing grid resolution required l_S be made proportional to source diameter rather than Δ. That requirement on l_S is not

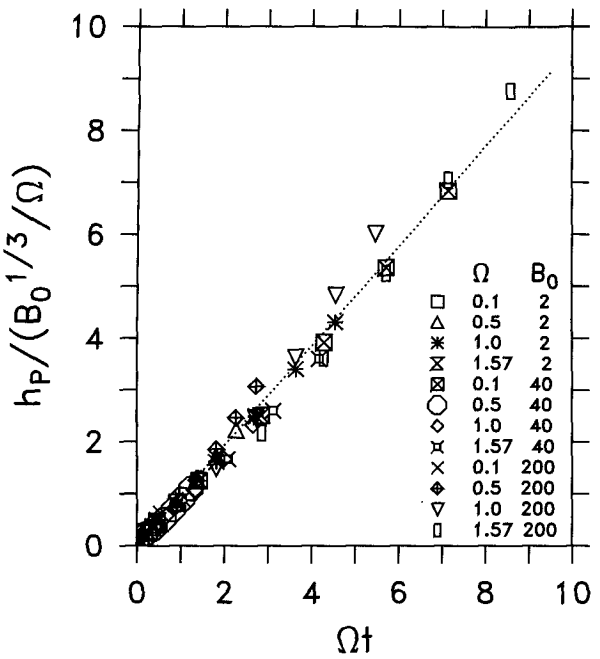

FIG. 5. Penetration depth h_P, nondimensionalized by the buoyancy flux B_0 and rotation rate Ω, as a function of nondimensionalized time. An analogous diagram in Fernando and Ching (1993) using data from laboratory experiments should be used for comparison. In the symbol table, B_0 is the actual value times 10^6 m^3 s^{-3}, and Ω has units of inverse seconds.

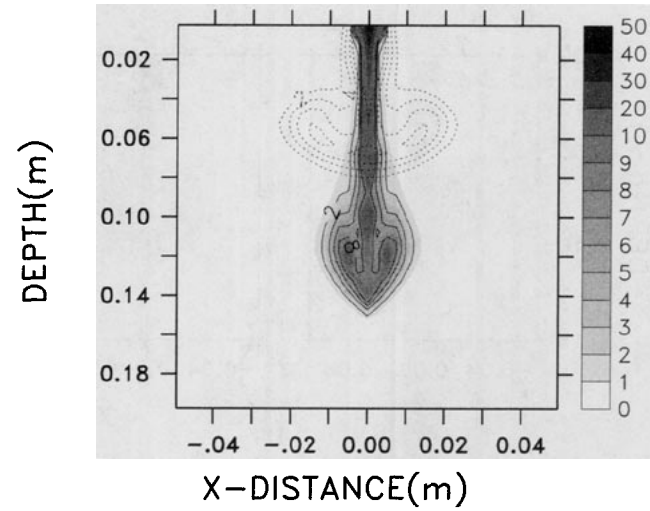

FIG. 6. Salinity distributions (‰) for two experiments differing only in the value of the Smagorinsky constant C_S. The deeper, narrower plume (shaded) results when $C_S = 0$, and the shallower, wider plume results when $C_S = 0.2$. In both cases, $\Omega = 0$, $B_0 = 40 \times 10^{-6}$ m^3 s^{-3}, $y = 0$, and $t = 2.35$ s.

entirely new. Sykes et al. (1986), for example, in numerically modeling jets entering a mean flow, used turbulence kinetic energy closure with l_S proportional to the lateral jet dimension. Likewise, Reynolds (1976) suggests that the eddy viscosity in jet problems be made proportional to jet width. Given that background on jets and plumes, we expected that making l_S equal to the plume source width would suffice.

While that choice was of correct magnitude, a further refinement bettered the correlation of data in Fig. 5. Initial model experiments with $l_S = b$ showed that w_P increased more quickly than the $B_0^{1/3}$ dependence required by the Fernando and Ching (1993) data. To slow plume penetration as B_0 grew, we decided to modulate the initial choice of $l_S = b$ by a function involving B_0. Since $B_0^{1/3}t$ is a natural length scale for turbulent convection in an unstratified fluid, we made $l_S = \gamma B_0^{1/3}$. By choosing $\gamma = 0.25$s, l_S was given a magnitude in each case close to the source width; specifically, the ratio of l_S to b was 0.4, 1.2, and 1.9 for the three B_0 values. The final form for l_S then resulted in the collinearity seen in Fig. 5. Tests of the usefulness of this l_S formulation for other point and line source plumes awaits additional data, model experiments, and their coanalyses.

Given the quadratic dependence of A_I on l_S [Eq. (6)] and the dependence of l_S on B_0, turbulent mixing explicitly intensifies with B_0. Distributions of A_I also confirmed that viscosities exceeded background values within and just slightly beyond each plume, with A_I largest in regions of largest shear. Taken together, the results lead us to conclude that spatially and temporally

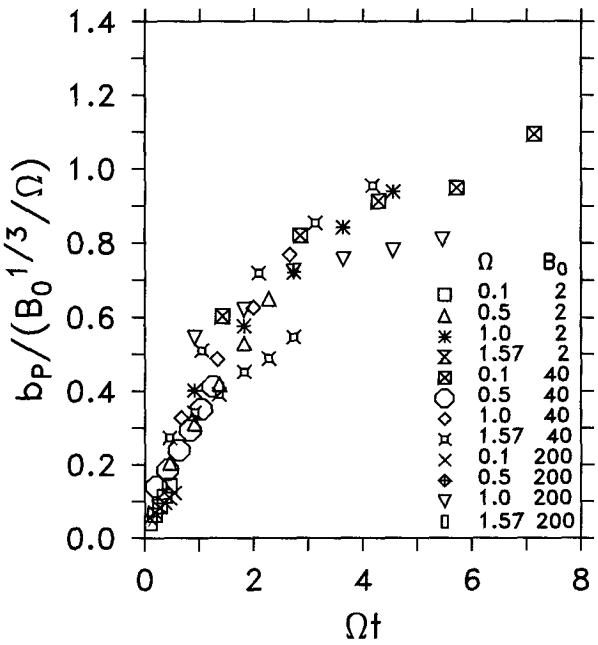

FIG. 7. Nondimensional half-width of the plumes at $y = 0$ as a function of nondimensional time. In the symbol table, B_0 is the actual value times 10^6 m^3 s^{-3}, and Ω has units of inverse seconds.

invariant subgrid-scale mixing coefficients are inadequate to the task of simulating these laboratory convection results over a range of buoyancy flux. In light of this, it is hard to envision any calculation of convection at geophysical scales that could do without shear-responsive subgrid-scale mixing of this or another type.

The nondimensional half-width of the plume cap $\tilde{b}_P$ has been plotted against time in Fig. 7 in a fashion similar to that for $\tilde{h}_P$. Some experiments at larger values of Ω did not contribute data, however, because a cap was not always well defined (e.g., Fig. 4d). Those that did show the initial growth of $\tilde{b}_P$ are nearly linear in time, but growth slows when $\Omega t \sim 2$. Since the source flux is steady here, the situation is different from point source thermal studies (Helfrich 1994) that show nondimensional width (not half-width) reached an asymptotic value of ~ 1 when $\Omega t \geq 2$. Figure 7 also shows that there is no critical time at which rotation first comes into evidence; Fernando and Ching (1993) noted that the rate of horizontal growth of plumes was greatly curtailed at approximately $\Omega t = 2.7$, but that was not obvious in our experiments. While $d(\tilde{b}_P)/dt$ generally slows in time, there is no sharp transition time. The much larger scatter for $\tilde{b}_P$ data (Fig. 7) compared with that for $\tilde{h}_P$ parallels experience with laboratory results (e.g., Helfrich 1994; Ayotte and Fernando 1994).

Fernando and Ching (1993) used measured plume depth and width at "time rotation becomes important" ($t = 2.7/\Omega$) to show that, at a fixed time, h_P and b_P vary as $B_0^{1/3}/\Omega$. We examined the possibility of that dependence at $t_R = 1/(2\Omega)$, not at their value of time because too few numerical experiments remained unaffected by bottom and end boundary effects than with the foreshortened tank depth we used. When $\log(h_P)$ and $\log(b_P)$, both values based on the 0.5% salinity isopleth, are plotted against $\log(B_0/\Omega^3 = (\mathrm{Ro}_C h)^3)$, distributions are seen to be linear (Fig. 8). Lines of 1/3 slope fit the data well (Fig. 8); dependence inferred is $h_P = 0.92(B_0/\Omega^3)^{1/3}$ and $b_P = 0.32(B_0/\Omega^3)^{1/3}$. Between laboratory and model results only the coefficients of the fit differ. Since Fernando and Ching (1993) evaluated h_P and b_P at a larger time, they reasonably found larger coefficients. The similarity of model (Figs. 5 and 8) and laboratory patterns (Fernando and Ching 1993) is quite good.

Why are plumes in environments with differing rotation rates so dissimilar (Fig. 4)? Velocity distributions in a plane perpendicular to the long axis and midway along the plume ($y = 0$) for two experiments differing only in Ω ($\Omega = 0.1$ and 1.57 s^{-1}, $B_0 = 40 \times 10^{-6}$ $m^3\ s^{-3}$) are very different (Fig. 9). For example, upward w (m s^{-1}) is large in the cap region and negligible above for small Ω (panel a), but w carries fluid upward within narrow flow zones all the way to the source level at larger Ω (panel b). For smaller Ω, maximum downward w, which is located in the recirculation region of the plume cap, is nearly twice that at the larger Ω (Figs. 9a and 9b).

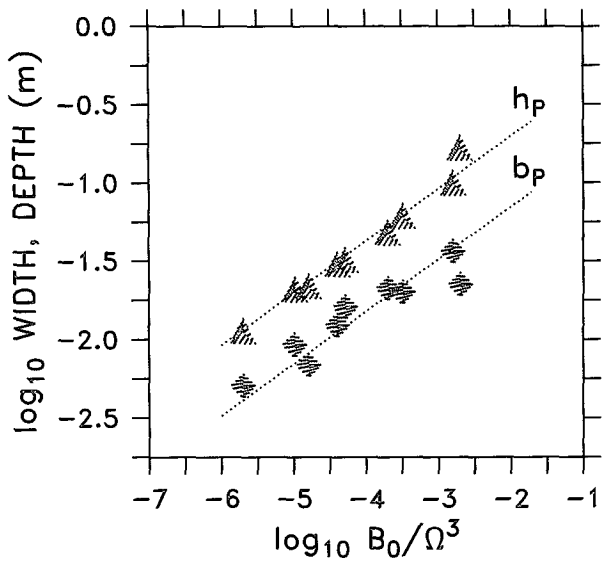

FIG. 8. Depth (triangles) and maximum half-width (squares) for plumes ($S = 0.5‰$ isopleth) at the time $t = (2\Omega)^{-1}$. Lines of slope 1/3 are fit to the data. Results should be compared to an analogous diagram from laboratory data by Fernando and Ching (1993). Some experiments provided no data for this plot as they were necessarily terminated before reaching $t = (2\Omega)^{-1}$.

At the high rotation rate, maximum ν exceeds that at smaller Ω by a factor of 5 (panels c and d), and the alongaxis (ν) flow extends well beyond the brine region as delineated by $S = 0.1‰$. Figure 9c shows little along-source velocity of any kind for the lower rotation rate case. The opposite is true at $y = 0$ for u velocities, with much stronger axis normal flow in the low rotation rate case. In both cases inflow near source level pinches the stem, but inflow there is stronger at smaller Ω (Figs. 9e and 9f). At the plume head, Figs. 9e and 9f show that u (at $y = 0$) is outward at smaller Ω and inward at larger Ω. The latter is favorable to restraining the plume lateral spread in the cap region. Distributions of u and w provide a recirculation regime that creates a broad plume cap in the first case and recirculates material upward on the periphery of the plume with little outward movement in the plume cap in the second (Fig. 4). Laboratory experiments for this source configuration have not yet provided velocity data.

When viewed on the plane $z = 4$ cm (Fig. 9g), other differences are apparent. At smaller Ω, u (contoured) is primarily transverse to the source axis, while at larger Ω substantial u (stippled) only occurs near the ends of the source. The opposite is true for ν (Fig. 9h). Horizontal velocities are more radial in both stem and cap at low Ω and more tangential to the plume, as might be expected, at higher Ω. What was unexpected was the

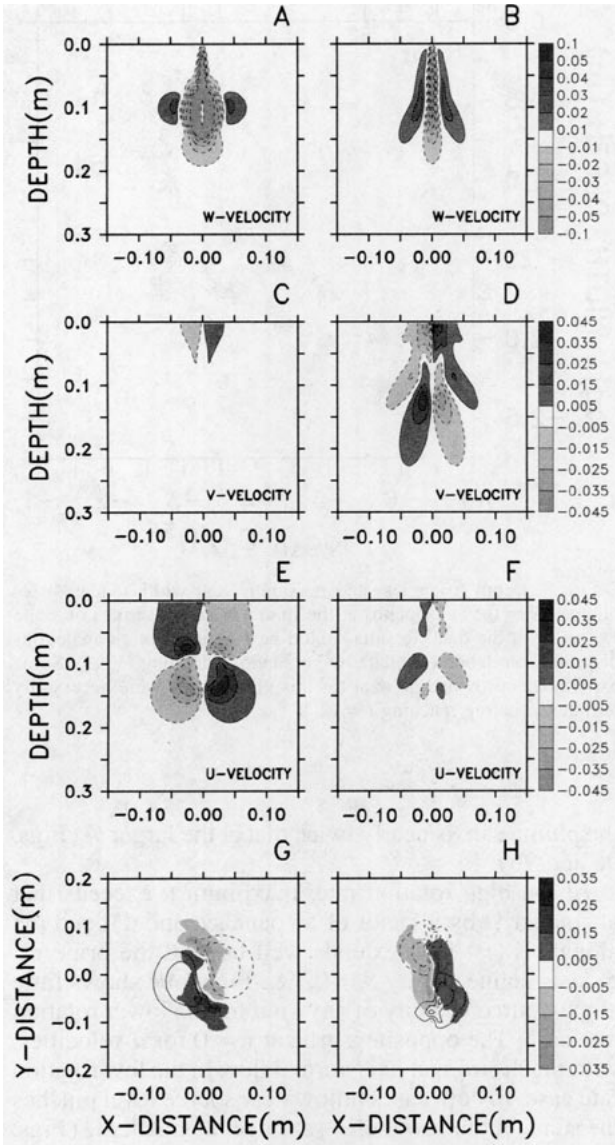

FIG. 9. Velocity distributions in meters per second at $t = 4.5$ s and $y = 0$ for two experiments [$\Omega = 0.1\ s^{-1}$, panels (a), (c), (e); $\Omega = 1.57\ s^{-1}$, panels (b), (d), (f); $B_0 = 40 \times 10^{-6}\ m^3\ s^{-1}$], the same cases depicted in Figs. 4a and 4d. At $z = 4$ cm, velocities u (panel g) and v (panel h) for the same two experiments are represented by line ($\Omega = 0.1\ s^{-1}$) and shaded ($\Omega = 1.57\ s^{-1}$) contours. Line contours in panels g and h have magnitudes of 0.005 and 0.015 m s^{-1}.

differences in vertical flow structure exhibited in Figs. 8a and 8b.

Are plume differences (e.g., Fig. 4) partly the result of changes in turbulent mixing caused by rotation, as speculated upon by Fernando and Ching (1993)? If the magnitude of the mixing coefficient can serve as an indicator, the answer is no. When $A_{V\,(\text{or}\,H)}$ [Eqs. (4)–(5)] is averaged over the region of the plume for which $S > 0.1‰$, $\langle A_V \rangle$ show a quick rise in time to asymptotic values, but little dependence on Ω (Fig. 10); the cluster of curves represent experiments with identical B_0 but differing Ω. Within each cluster the sequence of curves proceeds from the solid curve for $\Omega = 0.1\ s^{-1}$ to the chain-dot curve for $\Omega = 1.57\ s^{-1}$. The subgrid-scale formulation [Eqs. (4)–(10)] allowed implicit dependence of A_I on Ω via velocity gradients, but Fig. 10 shows that Ω exerts little influence on the turbulent mixing coefficient. For example, differences in maximum A_I over the four cases of Fig. 4 is at most 20%. On the other hand, mixing intensity depends significantly on B_0; A_I is as much as 130 times $A_{\min}$ for $B_0 = 200 \times 10^{-6}\ m^3\ s^{-3}$. Because resolved scale motions do not appear to have a chaotic component, we must conclude that differences in plumes (e.g., Fig. 4) under differing rotation rates are not the consequence of rotationally affected turbulence.

The present study was undertaken, in part, to examine the suitability of the subgrid-scale mixing parameterization, a task which could only be accomplished in the presence of actual data. The recent laboratory experiments (Fernando and Ching 1993) are important in this regard because, as best we are aware, comprehensive data for convection from line segment sources would not otherwise exist. The likeness of model and laboratory results (Figs. 5 and 8) support the choices made. While success with this mixing formulation scaled to geophysical problems is not guaranteed, it is unlikely that a mixing formulation that cannot address laboratory data on convection could be given much trust. From a geophysical prospective,

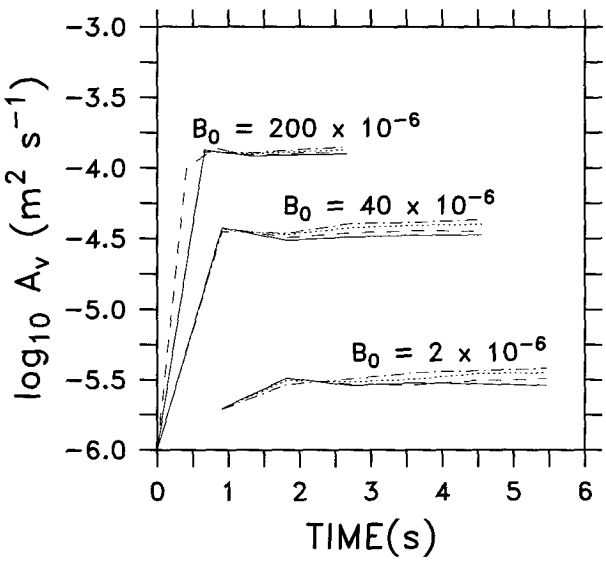

FIG. 10. Histories of average turbulent viscosity $A_V = A_H$ within the plume ($S > 0.1‰$). Clusters of curves represent experiments with identical B_0 but differing Ω. Within each cluster, the sequence of curves proceeds from the solid curve for $\Omega = 0.1\ s^{-1}$ to the chain-dot curve for $\Omega = 1.57\ s^{-1}$.

however, the utility of this same Smagorinsky–Lilly subgrid-scale mixing prescription has, in fact, been examined in the context of convection from point sources for which geophysical data is available, and comparisons of model and data have been encouraging (Lavelle and Baker 1994).

Can line segment convection at geophysical scales have any resemblance to these laboratory/model results? The answer appears to be yes. Application of this model, modified to permit background stratification, has been made to a seafloor fissure release of heat accompanying a magmatic event at a ridge crest spreading center (Lavelle 1995). That work suggests that with the event's buoyancy flux ($B_0 = 3.2 \times 10^{-2}$ m^3 s^{-3}) and earth's rotation rate ($\Omega = 7.29 \times 10^{-5}$ s^{-1}), one could expect a plume that rises to a density equilibrium level at ~900 m above the seafloor within a time period of 80 min and that within a time period of $\sim f^{-1}$ the plume will have begun to twist qualitatively in the manner of the plume depicted in Figs. 1 and 2. Those calculations also show $d(h_P)/dt \sim 0.75 B_0^{1/3}$ during the initial ascent in weakly stratified conditions. While some hydrographic observations of such plumes have been made (Baker et al. 1994), the density of observations in time and space is not adequate to substantiate specific features (e.g., Figs. 2 and 9) identified via the model.

4. Conclusions

Laboratory results on convection from line segment sources can be numerically simulated when nonlinear subgrid-scale mixing of the Smagorinsky–Lilly type is used to determine the time and space dependence of the turbulent mixing coefficients. Plume penetration speed was found to be dependent on the size of the turbulent mixing length l_S. Laboratory results were best described when l_S was given a 1/3 power dependence on source buoyancy flux. As a result, mixing coefficients changed in magnitude by two orders in response to buoyancy flux changes over the same range and were other than of background magnitude only in plume regions. Constant mixing coefficients of small size did not permit the same close resemblance of model and laboratory results. Moreover, only time- and space-variable A_H and A_V can account for the inhomogeneity of turbulent mixing within and beyond a plume. Thus, it is unlikely that a convection simulation that does not account for variations in the magnitude of subgrid-scale mixing can have the simulation fidelity that should be expected.

Effects of rotation in these simulations result from resolved-scale motion rather than from the subgrid scale. Little change in either maximum or average $A_{H,V}$ was evident under varying Ω. While rotation can affect homogeneous turbulence intensity under some conditions, rotation need not affect turbulence for effects of rotation on the flow to be evident in this convection context. Rotation very much affects all component velocities; upward transport at the periphery of the stem is much enhanced by rotation, resulting in a thickened plume stem and a slighter cap compared to the plume formed at smaller Ω. Flow tends to be inward or outward, depending on level, in both x and y directions under low rotation, but more tangential at high rotation.

Acknowledgments. Support for convection work for JWL comes from the NOAA VENTS program and for DCSIV from the Office of Naval Research.

REFERENCES

Ayotte, B. A., and H. J. Fernando, 1994: The motion of a turbulent thermal in the presence of background rotation. *J. Atmos. Sci.*, **51,** 1989–1994.

Baker, E. T., G. J. Massoth, R. A. Feely, R. E. Thomson, and B. J. Burd, 1995: Hydrothermal event plumes from the CoAxial seafloor eruption site. Juan de Fuca Ridge. *Geophys. Res. Lett.*, **22,** 147–150.

Bardina, J. R., J. H. Feziger, and R. S. Rogallo, 1985: Effects of rotation on isotropic turbulence: Computation and modeling. *J. Fluid Mech.*, **154,** 321–336.

Ching, C. Y., H. J. S. Fernando, and Y. Noh, 1993: Interaction of a negatively buoyant line plume with a density interface. *Dyn. Atmos. Oceans,* **19,** 367–388.

Clark, T. L., and R. D. Farley, 1984: Severe downslope windstorm calculations in two and three spatial dimensions using an elastic interactive grid nesting: A possible mechanism for gustiness. *J. Atmos. Sci.*, **41,** 329–350.

Drake, R. L., P. D. Coyle, and D. P. Anderson, 1974: The effects of nonlinear eddy coefficients on rising line thermals. *J. Atmos. Sci.*, **31,** 2046–2057.

Embley, R. W., W. W. Chadwick Jr., I. R. Johnson, D. A. Butterfield, and E. T. Baker, 1995: Initial results of the rapid response to the 1993 CoAxial Event: Relationships between hydrothermal and volcanic processes. *Geophys. Res. Lett.*, **22,** 143–146.

Fernando, H. J. S., and C. Y. Ching, 1993: Effects of background rotation on turbulent line plumes. *J. Phys. Oceanogr.*, **23,** 2125–2129.

——, R. R. Chen, and D. L. Boyer, 1991: Effects of rotation on convective turbulence. *J. Fluid Mech.*, **228,** 513–547.

Fofonoff, N. P., and R. C. Millard Jr., 1983: Algorithms for computation of fundamental properties of seawater. *UNESCO Tech. Papers in Mar. Sci.*, **44,** p. 53.

Galperin, B., and S. A. Orzag, Eds., 1993: *Large Eddy Simulation of Complex Engineering and Geophysical Flows.* Cambridge University Press, 600 pp.

Harlow, F. H., and J. E. Welch, 1965: Numerical calculation of time-dependent viscous incompressible flow of fluid with a free surface. *Phys. Fluids,* **8,** 2182–2189.

Helfrich, K. R., 1994: Thermals with background rotation and stratification. *J. Fluid Mech.*, **259,** 265–280.

Jones, H., and J. Marshall, 1993: Convection with rotation in a neutral ocean: A study of open-ocean deep convection. *J. Phys. Oceanogr.*, **23,** 1009–1039.

Lavelle, J. W., 1995: The initial rise of a hydrothermal plume from a line segment source: Results from a three-dimensional numerical model. *Geophys. Res. Lett.*, **22,** 159–162.

——, and E. T. Baker, 1994: A numerical study of local convection in the benthic ocean induced by episodic hydrothermal discharges. *J. Geophys. Res.*, **99,** 16 065–16 080.

Lilly, D. K., 1962: On the numerical simulation of buoyant convection. *Tellus,* **14,** 148–172.

Lipps, F. B., 1977: A study of turbulence parameterization in a cloud model. *J. Atmos. Sci.*, **34,** 1751–1772.

Mason, P. J., 1994: Large-eddy simulation: A critical review of the technique. *Quart. J. Roy. Meteor. Soc.,* **120,** 1–26.

——, and A. R. Brown, 1994: The sensitivity of large-eddy simulations of turbulent shear flow to subgrid models. *Bound.-Layer Meteor.,* **70,** 133–150.

Maxworthy, T., and S. Narimousa, 1994: Unsteady, turbulent convection into a homogeneous, rotating fluid, with oceanographic applications. *J. Phys. Oceanogr.,* **24,** 865–887.

Raash, S., and D. Etling, 1991: Numerical simulation of rotating turbulent thermal convection. *Beitr. Phys. Atmos.,* **64,** 185–199.

Reynolds, W. C., 1976: Computation of turbulent flows. *Ann. Rev. Fluid Mech.,* **8,** 183–208.

Roberts, P. J. W., 1979: Line plumes and ocean outfall dispersion. *J. Hydrol. Div.,* ASCE, **105,** 313–320.

Smagorinsky, J., 1963: General circulation experiments with the primitive equations. Part I. *Mon. Wea. Rev.,* **91,** 99–152.

——, 1993: Some historical remarks on the use of nonlinear viscosities. *Large Eddy Simulation of Complex Engineering and Geophysical Flows,* B. Galperin and S. A. Orzag, Eds., Cambridge University Press, 3–36.

Smith IV, D. C., and J. Morison, 1993: A numerical study of halocline convection beneath leads in sea ice. *J. Geophys. Res.,* **98**(C6), 10 069–10 084.

Strothers, R. B., 1989: Turbulent atmospheric plumes above line sources with an application to volcanic fissure eruptions on the terrestrial planets. *J. Atmos. Sci.,* **46,** 2662–2670.

Sykes, R. I., W. S. Lewellen, and S. F. Parker, 1986: On the vorticity dynamics of a turbulent jet in a cross flow. *J. Fluid Mech.,* **168,** 393–413.

Tag, P. M., F. W. Murray, and L. R. Koenig, 1979: Comparison of several forms of eddy viscosity parameterization in a two-dimensional cloud model. *J. Appl. Meteor.,* **18,** 1429–1441.

Tsang, G., 1970: Laboratory study of two-dimensional starting plumes. *Atmos. Environ.,* **4,** 519–544.

Woods, A. W., 1993: A model of the plumes above basaltic fissure eruptions. *Geophys. Res. Lett.,* **20,** 1115–1118.